Philosophical Magazine Letters,
Vol. 86, No. 12, December 2006, 829–835

An experimental investigation on a nanoporous carbon functionalized liquid damper

V. K. PUNYAMURTULA, A. HAN and Y. QIAO*

Department of Structural Engineering, University of California
at San Diego, La Jolla, CA 92093-0085, USA

(*Received 12 April 2006; in final form 25 September 2006*)

The behaviour of a *p*-xylene-based lyophobic nanoporous carbon system under high hydrostatic pressures is investigated. As the pressure is increased to a critical value, the nanopore surfaces between graphene layers are exposed to the liquid phase, leading to a considerable increase in solid–liquid interfacial energy. During unloading, defiltration does not occur until the pressure is much lower. Thus, the system is energy absorbing. Owing to the large solid–liquid contact area, the energy absorption efficiency is much higher than that of conventional dampers.

1. Introduction

Developing liquid dampers has been an active research area for many decades [1, 2]. First, owing to the high flexibility of the liquid phase, a liquid (as opposed to a solid) damper and the target, i.e. the structure to be protected, fit together well, maximizing the contact area and avoiding mismatches. Second, a liquid damper is usually lightweight and small sized, lowering the complexity of the system. Finally, the liquid phase can exhibit unique thermal, electric, magnetic and/or optical properties that are not obtainable using solid materials, providing important degrees of freedom for system design. Over the years, damping liquids in tanks [4, 5], liquid mounting stages [5], as well as liquid armour [6, 7] have been investigated, and many of them have received wide applications in industry.

However, currently, most of the dampers are based on non-energy-absorbing liquids, such as water. Therefore, as an external impact loading is applied, the compressive stress wave can only be redistributed and the decay in magnitude as it propagates across the liquid phase is negligible. The transmitted stress wave can cause serious damages in target structures, for example, the blast-lung problem [8–10]. Since most liquids, including shear-thickening liquids [11, 12], can dissipate energy only under shear loadings, to develop liquid dampers working under compressive loadings, new mechanisms must be employed.

Recently, Surani and co-workers [13–15] investigated a novel liquid-based damping system. As a hydrophobic nanoporous silica gel was added in water, when

---

*Corresponding author. Email: yqiao@ucsd.edu

Philosophical Magazine Letters
ISSN 0950-0839 print/ISSN 1362-3036 online © 2006 Taylor & Francis
http://www.tandf.co.uk/journals
DOI: 10.1080/09500830601064468

the hydrostatic pressure reached the critical value for overcoming the capillary effect, pressure-induced infiltration could take place in the nanopores. As most of the nanoporous space was filled, the large nanopore surfaces, with the specific area of $A = 278\,\mathrm{m}^2/\mathrm{g}$, were exposed to water. The excess silica–water interfacial tension, $\Delta\gamma$, which was defined as $\gamma_{\mathrm{sw}} - (\gamma_{\mathrm{w}} + \gamma_{\mathrm{s}})$, was around 50 mJ/m^2 [16], with γ_{sw} being the silica–water interfacial tension, γ_{w} the surface tension of water, and γ_{s} the surface tension of silica. Thus, the increase in specific silica–water interface energy was $\Delta U = \Delta\gamma \cdot A \approx 14\,\mathrm{J/g}$ – much higher than that of many conventional damping materials, such as reinforced polymers and shape-memory alloys. As the pressure decreases, the 'outflow' of the confined liquid in the nanopores was difficult, and ΔU was effectively dissipated.

One drawback of the above system is complications in preparation of the nanoporous silica gel, which consists of sophisticated template-formation, activation and surface-treatment steps. Moreover, compared with many other nanoporous materials, the surface area of the silica gel is relatively low, leaving considerable room for improvement. In view of these considerations, the current study investigates a nanoporous carbon, one of the earliest nanoporous materials used by humans. The nanoporous structure is formed by the imperfect packing and bending of graphene nanolayers [17]. Usually, they are synthesized by appropriate carburization treatment of organic materials, while a few deposition or nanocasting techniques have also been developed [18]. Nanoporous carbons are of pore sizes typically lower than 2 nm and pore surfaces of about $1000\,\mathrm{m}^2/\mathrm{g}$ – much larger than that of nanoporous silica gels. They are easy to synthesize, cost efficient and available in large volumes, ideal for developing large-scale dampers.

2. Experimental

The testing sample was produced by mixing 0.5 g of J. T. Baker E345-07 nanoporous carbon in 8.0 g of liquid phase. The as-received carbon was in powder form, with a particle size of about 20 µm and a specific surface area of $800\,\mathrm{m}^2/\mathrm{g}$. The liquid phase was chosen as Fluka 95682 *p*-xylene, a non-polar chemical with the molecular formula of $C_6H_4(CH_3)_2$ and a molecular weight of 106.17. Under ambient condition, the nanoporous carbon was non-wettable to *p*-xylene and, thus, the liquid cannot be absorbed into the nanopores spontaneously.

The carbon/*p*-xylene mixture was sealed in a steel cylinder, as shown in figure 1. Using a type 5569 Instron machine, a hydrostatic pressure, *p*, was applied on the liquid phase through the steel piston. The pressure was increased by moving the piston into the cylinder at a constant rate of 1 mm/min. The effective strain rate was at the level of 10^{-3}/s and, thus, the loading condition was quasi-static. Two sets of experiments of different maximum pressures were performed. In the low-pressure experiment, as the pressure exceeded 55 MPa, the piston was moved back at the same rate until the pressure was reduced to zero. In the high-pressure experiment, the pressure was increased to 155 MPa, followed by the unloading. In both sets of experiments, the loading–unloading process was repeated for more than six cycles. The measured sorption isotherm curves are shown in figures 2 and 3.

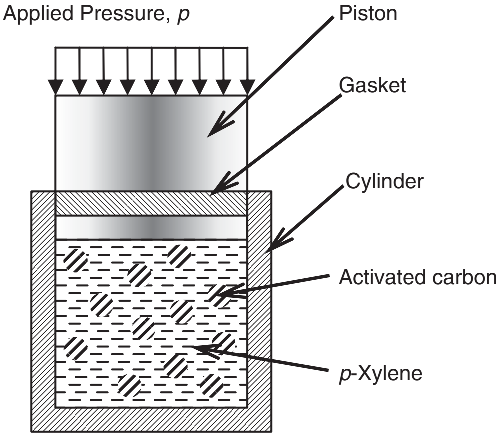

Figure 1. Schematic diagram of the nanoporous carbon functionalized liquid damper.

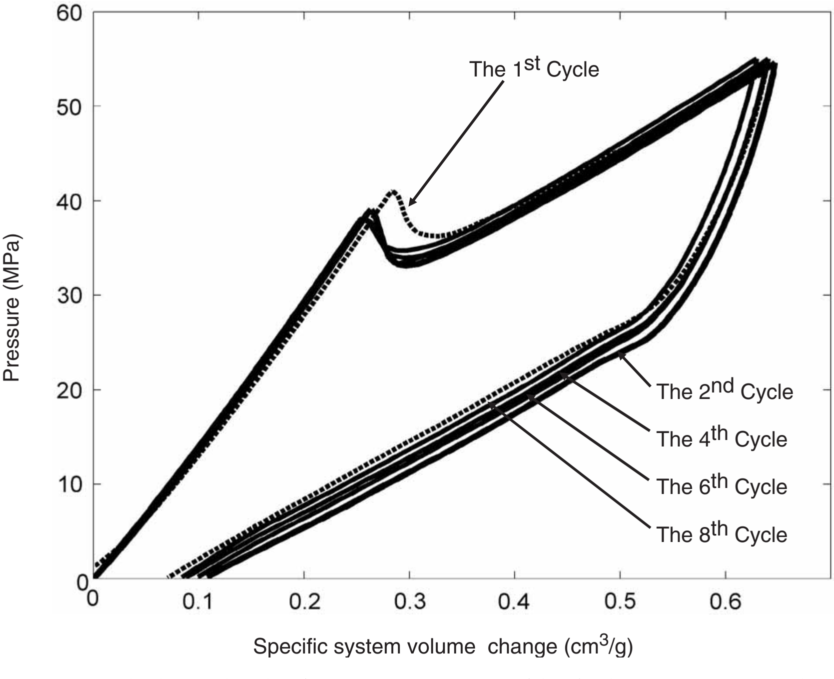

Figure 2. Typical sorption isotherm curves measured in the low-pressure experiment.

3. Results and discussion

Through figure 2, it can be seen that the nanoporous carbon works quite well under the cyclic loading. In the first loading–unloading cycle, as shown by the dashed line, the sorption isotherm curve is initially quite linear, indicating that *p*-xylene cannot

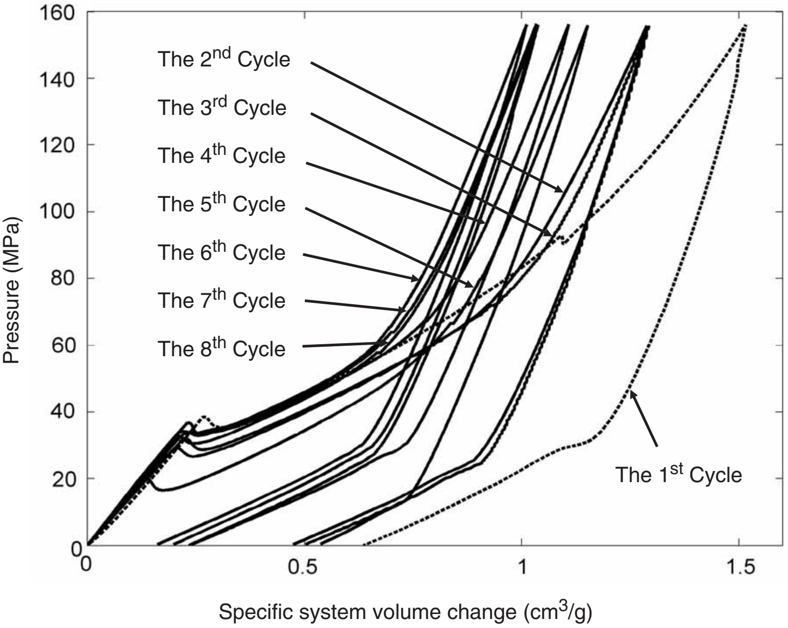

Figure 3. Typical sorption isotherm curves measured in the high-pressure experiment.

enter the nanopores if the pressure is relatively low. When the pressure reaches 41 MPa, the capillary effect of the largest nanopores is overcome and the liquid begins to infiltrate into the nanoporous particles. As the pressure increases, more and more smaller nanopores are involved in the pressure-induced infiltration and, consequently, an infiltration plateau is formed. The profile of the infiltration plateau is relatively linear, suggesting that the nanopore size distribution of the nanoporous carbon is parabolic.

As the pressure is lowered, similar to the phenomena of nanoporous silica [19, 20], the 'outflow' of the liquid in the nanopores is difficult. In other words, the confined liquid does not defiltrate unless the pressure is much lower than the infiltration pressure, which should be attributed to the confinement effect of nanopore walls and the mass and energy exchanges between gas and liquid phases in the nano-environment [21]. As the pressure is about 26 MPa lower than the infiltration pressure, the liquid starts to come out of the nanoporous particles, starting in the smallest nanopores, where the gas phase formation and growth is easier [21]. As the pressure is further decreased, liquid comes out of larger nanopores. The slope of the defiltration plateau is close to that of the infiltration plateau, indicating that, after defiltration starts, the defiltration behaviour can be regarded as the reversed process of infiltration; i.e. the unloading performance of the system is dominated by the initiation of defiltration. The specific dissipated energy, which can be calculated as the area enclosed by the loading–unloading loop, is 15 J/g.

Note that, immediately after the infiltration begins, there is a sudden drop in infiltration pressure, which should be related to the difficulty in pressure-induced nucleation of liquid phase in nanopores. As a liquid 'column' is formed in a nanopore, further intrusion becomes relatively easy, which is likely caused by the irregular shape of the nanopores of the carbon [17], somewhat similar with the irregular sorption isotherm curves observed in mercury porosimetry [23]. Furthermore, immediately after the unloading finishes, there is a ‘residual’ deformation. However, this deformation vanishes quickly in the low-pressure experiment, before the second loading is applied. In other words, the system nominally returns to the initial configuration and, therefore, in the following loading–unloading cycles the energy absorption procedure can be repeated, as shown by the solid lines in figure 2. Hence, this system can work continuously, having great potential for developing advanced damping systems, such as earthquake-proof foundations, vibration-proof stages and layers, etc. Compared with the first infiltration–defiltration loop, the following loops are of slightly lower infiltration pressures. On the other hand, the variation in the width of infiltration plateau is negligible, suggesting that during the first loading–unloading cycle the smallest nanopores are combined with adjacent nanoporous structures, probably due to the high local capillary pressure.

In the experiment discussed above, the nanopore volume of the nanoporous carbon is not fully utilized, since the maximum pressure is only about 55 MPa, insufficient to overcome the capillary effect of the smallest nanopores. If the maximum pressure is increased to 155 MPa, as shown in figure 3, the width of the infiltration plateau increases considerably, indicating that most of the nanopores, including those not involved in the low-pressure infiltration, are intruded by the liquid. The profile of the first-cycle sorption isotherm curve is somewhat similar to that of figure 2, while the infiltration plateau width is 1.25 cm^3/g – close to the total nanopore volume – leading to an improved energy absorption efficiency of 49 J/g.

From the second loading–unloading cycle, the system behaviour changes significantly. For instance, the infiltration plateau widths of the second and the third cycles are only about 75% of the first cycle. The infiltration plateau width of the fourth cycle is only about 60%. In the fifth cycle, while the width of the infiltration plateau is larger, the infiltration pressure is only about 65% of the first cycle. This pattern is not maintained in the sixth and the seventh cycles, where the infiltration pressures are higher yet the infiltration plateau widths are smaller. In other words, the sorption isotherm curves become highly irregular. Clearly, the nanoporous structure is damaged during the high-pressure infiltration process. The decreases in accessible pore volume indicates that the nanopores collapse and the decrease in infiltration pressure suggests that the collapsed nanopores are those of smallest sizes, which is in agreement with the fact the capillary pressure increases as the pore size decreases. The occasional increase in accessible pore volume indicates that nanopore reopening can also take place, which should be caused by the change in packing mode of graphene nanolayers. Specifically, as the porosity decreases to a certain level, the close-packed graphene nanolayers are relatively unstable and, therefore, can break down into nanoporous structures as a high external pressure is applied. However, such an additional porosity process is unrepeatable and, thus, should be regarded as a random factor. Under this condition, after the first loading–unloading cycle, the energy absorption efficiency of the system is not only smaller but also unreliable. Hence, for the design of protective devices, only the first loading should be taken into consideration and the system is suitable only for one-time use, such as car bumpers and body armour.

4. Conclusions

The energy absorption behaviour of a nanoporous carbon immersed in *p*-xylene is investigated. As pressure increases, the non-wetting liquid can be forced into the energetically unfavourable nanopores, leading to a significant increase in system free energy. Since the sorption isotherm curve is hysteretic, the free energy cannot be fully released as the pressure is lowered; i.e. a considerable portion of the external work is dissipated. For low-pressure applications, the nanoporous structure is quite stable and the system can work continuously under a cyclic loading, with the damping efficiency at the level of 15 J/g. For high-pressure applications, the nanoporous structure is damaged due to the high capillary pressure in the smallest nanopores and, therefore, only the system response at the first loading is reliable. Under this condition, the system should be used only for one-time applications, with the energy absorption efficiency at the level of 50 J/g.

Acknowledgements

This study was supported by The Air Force Office of Scientific Research under Grant No. FA9550-06-1-0181, for which the authors are grateful to Dr. Byung-Lip Lee.

References

[1] G. Lu and T. Yu, *Energy Absorption of Structures and Materials* (CRC Press, Boca Raton, FL, 2003).
[2] E.I. Rivin, *Stiffness and Damping in Mechanical Design* (Marcel Dekker, New York, 1999).
[3] I. E. Sumner, *An Experimental Investigation of the Viscous Damping of Liquid Sloshing in Spherical Tanks*, (NASA Technical Note, Cape Canaveral, FL, 1963).
[4] F. T. Dodge, *Moment of Inertia and Damping of Liquids in Baffled Cylindrical Tanks*, (NASA Technical Note, Cape Canaveral, FL, 1966).
[5] J.L. Barrat and J.P. Hansen, *Basic Concepts for Simple and Complex Liquids* (Cambridge University Press, New York, 2003).
[6] Y.S. Lee, E.D. Wetzel and N.J. Wagner, J. Mater. Sci. **38** 2825 (2003).
[7] A.R. Raffray, S.I. Abdel-Khalik, D. Haynes, *et al.*, Fusion Sci. Technol. **46** 438 (2004).
[8] J.B. Hull, Br. J. Surg. **79** 1303 (1992).
[9] B. Hirshberg, A. Oppenheim-Eden, R. Pizov, *et al.*, Chest **116** 1683 (1999).
[10] V. Avidan, M. Hersch, Y. Armon, *et al.*, Am. J. Surg. **190** 927 (2005).
[11] J. Delhommelle and J. Petravic, J. Chem. Phys. **123** 074707 (2005).
[12] P. Hebraud and D. Lootens, Mod. Phys. Lett. B **19** 613 (2005).
[13] F.B. Surani, X. Kong, D.B. Panchal, *et al.*, Appl. Phys. Lett. **87** 163111 (2005).

[14] F.B. Surani, X. Kong and Y. Qiao, Appl. Phys. Lett. **87** 251906 (2005).
[15] F.B. Surani and Y. Qiao, J. Appl. Phys. **100** 014308 (2006).
[16] X. Kong and Y. Qiao, Appl. Phys. Lett. **86** 151919 (2005).
[17] S. Polartz and B. Smarsly, J. Nanosci. Nanotechnol. **2** 581 (2002).
[18] A. Dabrowski, Adv. Colloid Interface Sci. **93** 135 (2001).
[19] X. Kong, F.B. Surani and Y. Qiao, J. Mater. Res. **20** 1042 (2005).
[20] X. Kong and Y. Qiao, Phil. Mag. Lett. **85** 331 (2005).
[21] X. Kong and Y. Qiao, J. Appl. Phys. (2006), to be published.
[22] S. Snook, Euro. Autom. Design **5** 30 (2001).
[23] G. T. Shaw, *Porpsimetry by Mercury Injection* (CANMET, Ottawa, Canada, 1963).